Chemical Science

Accepted Manuscript

This article can be cited before page numbers have been issued, to do this please use: W. Huang, C. Wei, M. Wang, Q. Zhang and Z. He, *Chem. Sci.*, 2026, DOI: 10.1039/D6SC01341D.

ROYAL SOCIETY OF CHEMISTRY

rsc.li/chemical-science

View Article Online
DOI: 10.1039/D6SC01341D

ARTICLE

Efficient Red Circularly-Polarized Phosphorescence from Pyrene Derivatives Mediated by Locked Axial Chirality Scaffold

Received 00th January 20xx,
Accepted 00th January 20xx

DOI: 10.1039/x0xx00000x

Wenbin Huang,[a+], Chenlong Wei,[a+], Meng Wang,[a], Qian Zhang,[a] and Zikai He*[a]

As a classic polycyclic aromatic hydrocarbon luminophore, pyrene exhibits considerable potential for optoelectronic applications yet faces challenges in achieving chiral luminescence, particularly long-lived red circularly polarized phosphorescence. In this work, we report a strategy for manipulating the axial chirality of binaphthalene to enable pyrene to achieve efficient circularly polarized luminescence and red circularly polarized phosphorescence. It is revealed that the locked axial chiral binaphthalene not only boosts overall intersystem crossing via its transient triplet excited state but also amplifies circularly polarized phosphorescence through mediating structural rigidity and transition dipole moments. Bright circularly polarized luminescence with a high quantum yield of 65.7 % and distinct red circularly polarized phosphorescence with a dissymmetry factor of 6.5×10^{-3} and a persistent lifetime of 381.9 ms, are obtained. The outlined structure-property relationship provides insights into the design principle for developing efficient circularly polarized luminescent materials.

Introduction

Red circularly polarized phosphorescence (CPP) is a highly desirable property for biological imaging, environmental sensing, and three-dimensional displays[1-4] benefiting from its synergistic advantages of deep tissue penetration, unique chiral optics, and long-lived afterglow[5-11]. However, achieving efficient red CPP remains a formidable challenge[1, 12-14]. First, the inherently small energy gap between the triplet excited state (T_1) and the ground state (S_0) for red-light emission promotes nonradiative decay, leading to severe phosphorescence quenching[15]. Second, the large energy gap between the singlet excited state (S_1) and the T_1 state hinders efficient intersystem crossing (ISC), which is essential for populating the phosphorescent triplet state[16-18]. Third, in chiral systems, flexible molecular frameworks often lead to rapid relaxation of chiral excited states, thereby weakening circularly polarized light emission[19-22]. These fundamental limitations collectively impede the development of high-performance red CPP materials, necessitating the exploration of novel molecular design strategies[23-29].

Pyrene, a typical polycyclic aromatic hydrocarbon luminophore, has attracted significant attention as a building block for developing luminescent materials due to its high fluorescence quantum yield and tunable π-conjugated planar structure [30]. However, the lack of chirality in pyrene limits its applications in chiral optoelectronics, for instance, circularly polarized emission[31]. Additionally, pyrene-based materials usually exhibit strong fluorescence but weak phosphorescence, which limits their applications in bioimaging and information encryption that require long-lived luminescent signals[32-36]. Thus, several strategies have been attempted to introduce chirality into pyrene derivatives, including attaching chiral side chains[37-41] and constructing chiral supramolecular assemblies[42-45], but these approaches often suffer from weak chiral influence, poor stability of chiral structure, inefficient ISC, and inferior phosphorescence[46-48]. For example, chiral side chain modification introduces weak chiral induction, resulting in a low dissymmetry factor. Chiral supramolecular assemblies rely on non-covalent interactions, which are sensitive to external conditions and exhibit poor structural stability and reproducibility. Meanwhile, these strategies can only introduce chirality but cannot simultaneously improve ISC efficiency and phosphorescence performance. This urgently necessitates the development of novel molecular construction strategies to overcome the limitations.

Herein, we have successfully developed a novel strategy to achieve efficient circularly polarized luminescence (CPL) and red CPP from two pyrene derivatives (ONPY and CNPY) by manipulating the axial chirality of the binaphthalene skeleton (Scheme 1). By investigating the photophysical properties of pyrene, binaphthalene, ONPY, and CNPY, we systematically depicted the effects of open and locked axial chirality on the luminescent behavior of pyrene derivatives. They not only enhance intersystem crossing via the mediation of the transient triplet excited state of the chiral center but also amplify chiral emission by fixing the relative orientation of the pyrene and binaphthalene moieties and reducing conformational changes. Specifically, when doped into poly(vinyl pyrrolidone) (PVP), CNPY exhibits bright CPL with a $|g_{lum}|$ of 7.4×10^{-3} and a Φ_{PL} of 65.7 %, as well as distinct red-CPP with a $|g_{lum}|$ of 6.5×10^{-3} and a τ_P of 381.9 ms.

[a] College of Frontier Sciences, Harbin Institute of Technology, Shenzhen, Shenzhen 518055, China
[+] These authors contributed equally.
Supplementary Information available: [details of any supplementary information available should be included here]. See DOI: 10.1039/x0xx00000x

View Article Online
DOI: 10.1039/D6SC01741D

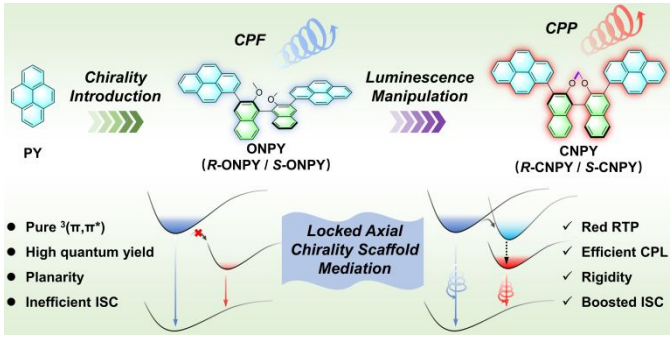

Scheme 1 | Diagram of molecular structural engineering and strategy for manipulating the locked axial chirality of binaphthalene to enable pyrene efficient circularly-polarized fluorescence (CPF) and red circularly-polarized phosphorescence (CPP).

Results and discussion

Molecular design and synthesis

Two derivatives were designed and synthesized: open axial chiral naphthalene-pyrene scaffold (ONPY) and locked axial chiral naphthalene-pyrene scaffold (CNPY)[49, 50]. The difference lies in the presence of a bridging group in CNPY that locks the axial chirality of the binaphthalene unit, while ONPY has no such bridging group, resulting in a flexible axial chirality (Scheme 1). The pure enantiomers, namely, *R*-ONPY, *S*-ONPY, *R*-CNPY, and *S*-CNPY, were prepared from commercially pure binaphthalene starting materials (Scheme S1, ESI†). The synthetic procedures and the corresponding structural characterization (^{1}H NMR, ^{13}C NMR, high-resolution mass spectrum) details are summarized in the Electronic Supplementary Material. The chiral high-performance liquid chromatography show that all enantiomers achieve separation, and the optical purity of each enantiomer is greater than 99% (*ee* > 99%) (Chart S7, ESI†).

Photophysical properties

The UV-visible absorption spectra in Figure 1a reveal distinct electronic transitions. Pyrene (PY) exhibits characteristic absorption bands at 300-350 nm, corresponding to the π-π* transition of $S_0 \rightarrow S_2$ based on its conjugated aromatic backbone[51]. Since the S_0 and S_1 states have the same symmetry, transitions between states with identical symmetry are forbidden in accordance with the symmetry selection rule for electronic transitions, and thus the $S_0 \rightarrow S_1$ absorption band cannot be detected. For ONPY and CNPY, the absorption bands corresponding to PY segments bathochromically shift to 300-380 nm due to increased molecular π-conjugation with binaphthalene (NA), with CNPY showing a more pronounced enhancement of absorption coefficient but a slightly higher-energy absorption edge than that of ONPY. It indicates that the locked skeleton in CNPY induces molecular rigidification and conjugation from the binaphthalene framework to the pyrene moieties, leading to an improved Frank-Condon factor.

The photoluminescence (PL) spectra in Figure 1b provide insights into photophysical properties. At room temperature in 2-MeTHF solutions, PY and NA emit deep blue fluorescence with peaks at 378 nm and 363 nm, respectively, whereas ONPY and CNPY show red-shifted fluorescence emission peaks at 390 nm and 392 nm, respectively. Upon cooling to 77 K (frozen matrix), all luminophores retain prompt fluorescence with more distinct vibrational profiles. The nanosecond lifetimes monitored at 400 nm proved their fluorescence nature. Several new red-shifted emission bands emerge, spanning 570 to 750 nm for PY, 380 to 700 nm for NA, and 380 to 750 nm for ONPY and CNPY, respectively. They are attributed to phosphorescence based on their millisecond-decay curves in Figure 1e. Notably, the phosphorescence of ONPY and CNPY is primarily derived from the pyrene fragment (575-700 nm) and secondarily from the binaphthalene fragment (475-575 nm), as identified by the wavelength and vibrational characteristics of their respective spectral profiles, while their fluorescence is entirely derived from the pyrene fragment. Moreover, compared to PY, ONPY and CNPY exhibit much more intense and persistent red phosphorescence, suggesting that superior intersystem crossing and phosphorescence efficiency are achieved in ONPY and CNPY. PL performance was successfully mediated by the chiral center, as evidenced by the observed phosphorescence from the binaphthalene segment. The longer fluorescence and phosphorescence lifetimes of CNPY indicate that the locked structure enhances structural rigidity, thereby weakening nonradiative transitions and further improving the luminescent performance.

The chiroptical properties of pure enantiomers are first characterized by circular dichroism (CD) spectroscopy. As shown in Figure 1d, all chiral enantiomeric derivatives exhibit mirror-imaged CD signals. Distinct alternating positive and negative Cotton effects are observed at 240-380 nm, which match well with their absorption bands. Careful investigation of the intensity and direction of CD signals reveals that the axial chiral binaphthalene skeleton induces obvious chiroptical absorption behaviours in pyrene segments. Meanwhile, the locked structure results in a higher CD intensity. The calculated g_{CD} of the CNPY enantiomers is higher than that of ONPY (Figure S2, ESI†). It indicates that in the ground state, the flexible configuration in ONPY results in a weak chiral response, whereas fixing the orientation of pyrene and binaphthalene skeletons induces a more pronounced chiroptical effect.

The CPL properties of enantiomers were then investigated to evaluate the effect of locked axial chirality on the luminescence. The CPL magnitude is assessed by the dissymmetry factors of g_{lum}, which are defined as $g_{lum} = 2\times(I_L-I_R)/(I_L+I_R)$, where I_L and I_R indicate the intensity of Left-CPL and Right-CPL, respectively. Figures 2a and 2b show the CPL spectra and g_{lum} in the fluorescence region at room temperature and 77 K, respectively. At room temperature, *R*-ONPY and *S*-ONPY show weak CPL signals with a quite low $|g_{lum}|$ of approximately 3×10^{-4}. In contrast, *R*-CNPY and *S*-CNPY exhibit slightly higher CPL signals with a $|g_{lum}|$ of approximately 4×10^{-4}. The $|g_{lum}|$ enhancement in CNPY enantiomers is probably attributed to structural rigidity induced by locked axial chirality and is conducive to stabilizing

View Article Online
DOI: 10.1039/D6SC01341D

ARTICLE

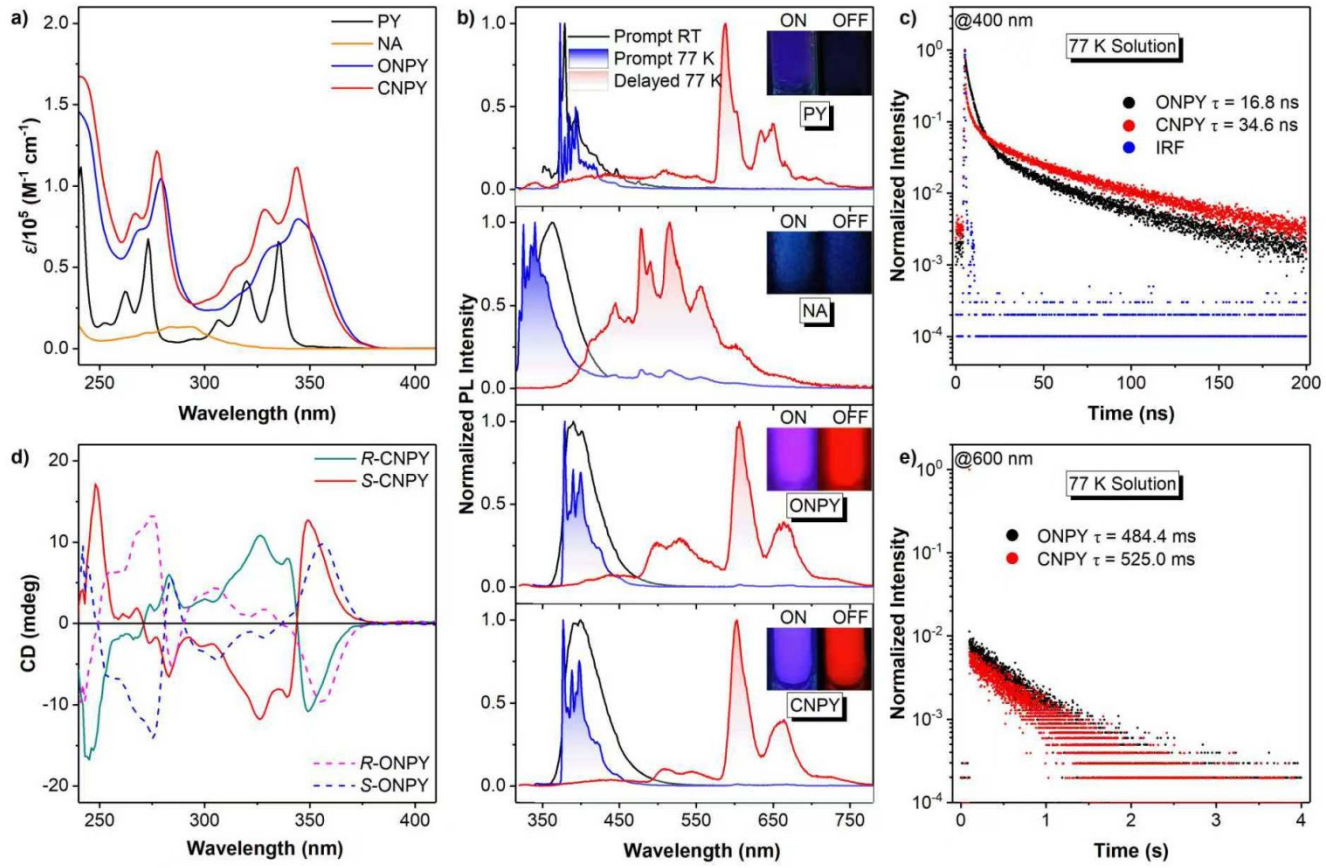

Figure 1 | (a) UV-visible absorption spectra of pyrene (PY), binaphthalene (NA), ONPY, and CNPY solutions (10^{-5} M) at room temperature (RT); (b) normalized prompt PL spectra in solution at RT, and normalized prompt PL and delayed (1 ms) spectra in solution at 77 K for PY, NA, ONPY and CNPY, respectively; Time-resolved (c) fluorescence and (e) phosphorescence decay curves and their respective lifetimes for ONPY and CNPY in solution at 77 K; (d) circular dichroism spectra in solution at RT for *R*-CNPY, *S*-CNPY, *R*-ONPY, *S*-ONPY, respectively.

the molecular conformation at the excited states.

Lowering the temperature to 77 K, there is further enhances in the CPL intensity of both enantiomers, with CNPY maintaining a higher $|g_{lum}|$ (8.9×10^{-3}) than ONPY (3.3×10^{-3}). It is found that the $|g_{lum}|$ of CNPY at 77 K is about 20 times that measured at room temperature, whereas the corresponding ratio for ONPY is about 8. The programmed enhancement of $|g_{lum}|$ provides compelling evidence that environmental confinement and conformational restriction facilitate the amplification of CPL. Notably, CNPY enantiomers achieve detectable CPL in the red phosphorescence region (580-700 nm) at 77 K (Figure 2c), with a $|g_{lum}|$ of about 10^{-2}, while ONPY enantiomers show no measurable CPP. It is an impressive result, as it demonstrates that a locked axial chiral scaffold not only boosts the ISC channel to populate triplet excitons but also effectively transfers the chirality of the binaphthalene framework to the triplet states of the pyrene fragments, enabling CPP emission.

Theoretical Calculations

To clarify the mechanism of locked axial chirality in regulating the photophysical (chiroptical) properties, we performed theoretical calculations. Figure 3 (Left) presents the results of state-energy-level diagrams, spin-orbit coupling (SOC) coefficients (ξ), and natural transition orbitals (NTOs) of ONPY and CNPY, respectively. Compared to the PY (Figure S4, ESI†), both ONPY and CNPY exhibit a smaller singlet-triplet energy gap (ΔE_{ST}) between S_1 and T_1 (1.300 eV for ONPY, 1.322 eV for CNPY, and 1.651 eV for PY). Multiple accessible intersystem crossing pathways (7 channels for ONPY and CNPY versus 4 ones for PY), as well as higher spin-orbit coupling coefficients, are obtained,

View Article Online
DOI: 10.1039/D5SC01341D

which should be responsible for the superior phosphorescence performance in ONPY and CNPY.

A detailed analysis of NTOs reveals that the axial chiral binaphthalene moiety is involved in the overall excited-state relaxation process, supporting intermediate triplet states (T_3 and T_4)[52, 53]. It is consistent with experimental PL spectra in Figure 1b. Furthermore, the axial chiral binaphthalene skeleton introduces the distorted excited-state configurations, which enable the circumferential migration of electrons between the π-orbitals of the twisted aromatic segments, employing the analogous El-Sayed's rule[54]. The distorted configuration mixes singlet and triplet states to facilitate exciton exchange and spin-flip, and separates pyrene to prevent intramolecular excimer formation[55, 56]. Meanwhile, the pure (π,π*) characteristics in T_1 of CNPY contribute to its persistent phosphorescence lifetime at 77 K. Overall, the binaphthalene scaffold mediates the phosphorescence properties.

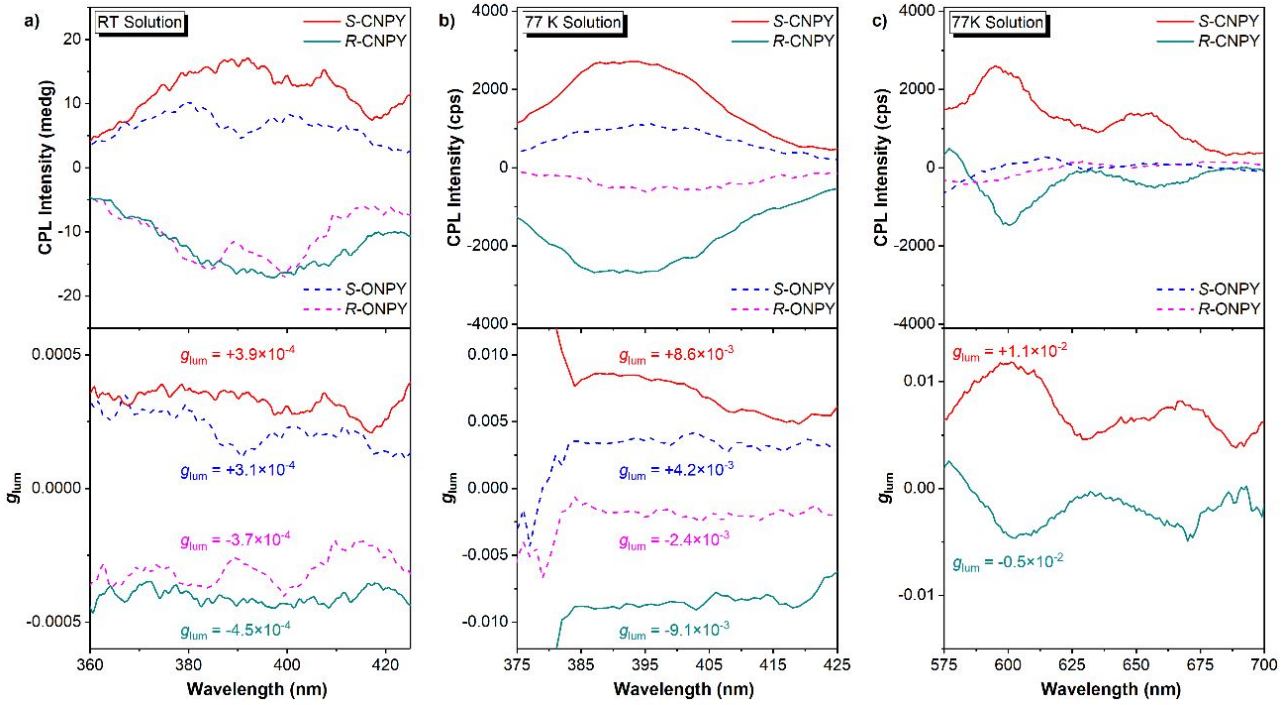

Figure 2 | CPL spectra (Top) and emissive dissymmetry factor g_{lum} (Bottom) of *S*-CNPY, *R*-CNPY, *S*-ONPY, *R*-ONPY solutions in 2-MeTHF, (a) the fluorescence region (360-425 nm) at room temperature, (b) at 77 K, (c) the phosphorescence region (575-700 nm) at 77 K.

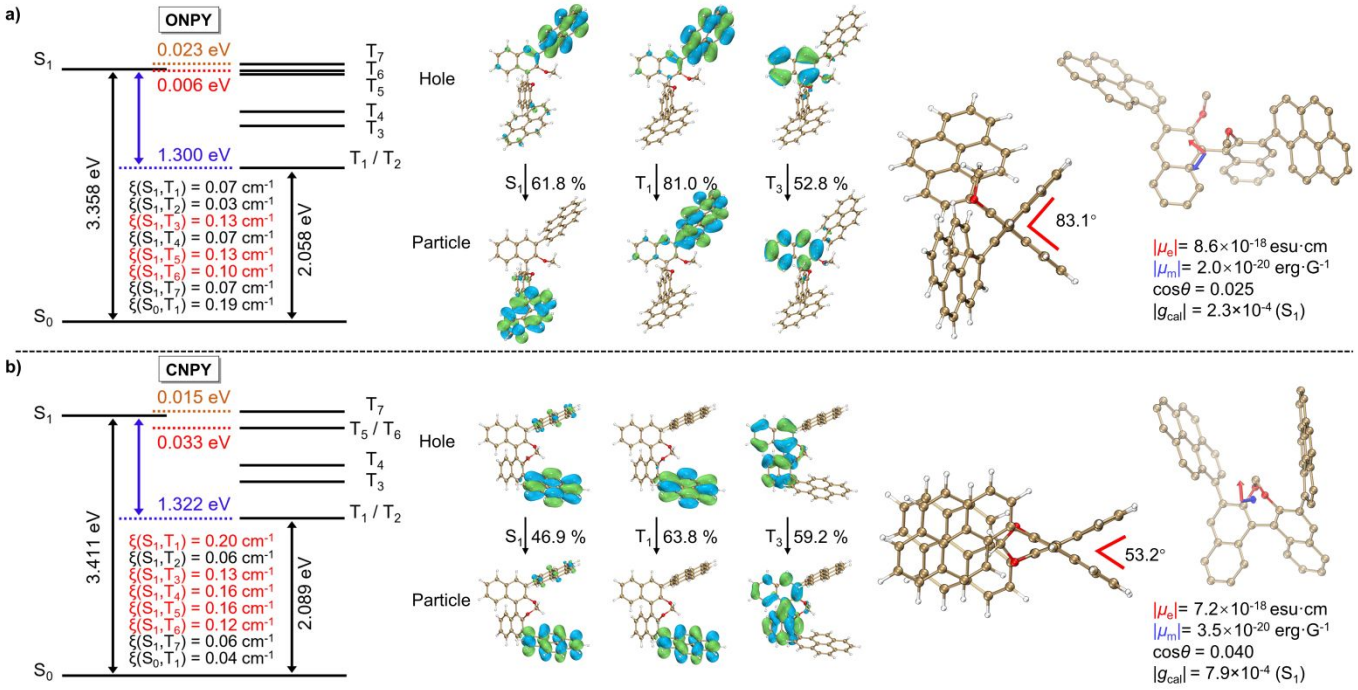

Figure 3 | The calculated state-energy diagrams, the SOC coefficients (ξ), NTOs, optimized molecular structures, the simulated electric (μ_e) and magnetic (μ_m) transition dipole moments, and calculated g_{cal} for singlet states of (a) ONPY and (b) CNPY in their monomeric state, respectively.

View Article Online
DOI: 10.1039/D6SC01341D

Additionally, we selected the representative *S*-ONPY and *S*-CNPY for excited-state geometry optimization and CPL simulation. As shown in Figure 3 (Right), the molecular configuration of *S*-ONPY is highly twisted, with a calculated dihedral angle of approximately 83.1° for the binaphthalene skeleton. In contrast, the dihedral angle of the locked binaphthalene skeleton in *S*-CNPY is 53.2°, significantly constraining the molecular geometry and providing superior structural rigidity. Based on these optimized structures, their electric transition dipole moments ($|\mu_e|$), magnetic transition dipole moments ($|\mu_m|$), and the intersection angles (θ) are calculated. Then, the dissymmetry factor g_{cal} are defined as $g_{cal} = (4\cos\theta|\mu_e||\mu_m|)/(|\mu_e|^2+|\mu_m|^2) \approx (4\cos\theta|\mu_m|)/|\mu_e|$. As a result, *S*-CNPY has a higher $|g_{cal}|$ of 7.9×10^{-4}, being approximately 3.4 times that of *S*-ONPY (2.3×10^{-4}). It is in agreement with the results obtained in 2-MeTHF solutions, indicating the positive effect of locked axial chirality in CNPY.

Circularly polarized room temperature phosphorescence

To evaluate the practical application potential, PY, ONPY, and CNPY were doped into a PVP matrix, and their photophysical properties were characterized at ambient conditions. PVP possesses abundant amide groups, which can restrict molecular motions via hydrogen bonding and van der Waals interactions with the dopant molecules. Meanwhile, its excellent solubility ensures uniform dispersion of the molecules and the dense film morphology. Also, we optimize the doping ratio and subject the resulting films to photo-thermal treatment before conducting photophysical measurements (Figure S5, ESI †). The results demonstrate that the 1:500 doping ratio is the best condition. An excessively low doping ratio results in a significant decrease in afterglow brightness, while an overly high ratio induces excimer formation and subsequent phosphorescence quenching. Moreover, the phosphorescence of the films treated by photothermal treatment was significantly enhanced. FTIR analysis confirms the structural changes induced by photo-thermal treatment (Figure S6, ESI†). The broad O–H/N–H vibrations at 3400 cm^{-1} are notably narrowed and weakened, indicating efficient removal of residual solvent and water. The strong C=O vibration at 1635 cm^{-1} is remarkably reduced, reflecting enhanced intermolecular hydrogen bonding between the dopant and PVP carbonyl groups. Additionally, the aromatic C=C (1421-1497 cm^{-1}) and C–H out-of-plane bending (645 cm^{-1}) peaks become sharper, demonstrating improved molecular dispersion and conformational rigidity of the dopant in the PVP matrix. These changes collectively establish a strong hydrogen-bonded network and suppress non-radiative vibrational relaxation, providing a structural foundation for enhanced phosphorescence and circularly polarized luminescence performance.

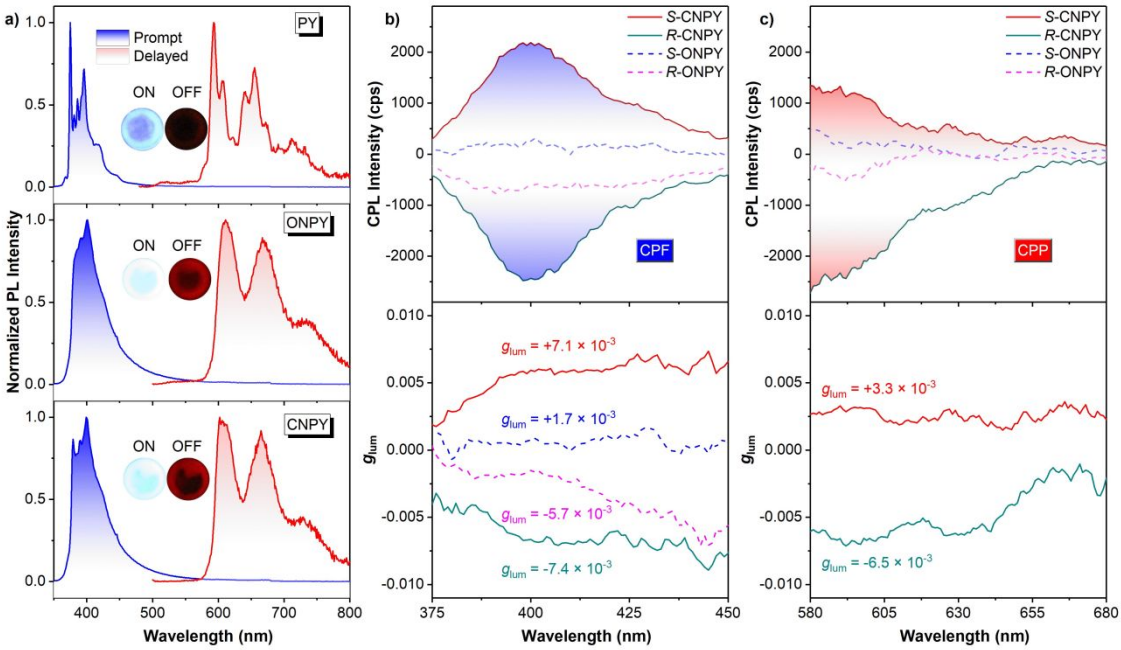

Figure 4 | (a) Normalized prompt and delayed (1 ms) PL spectra in PVP films at room temperature for PY, ONPY, and CNPY, respectively. CPL spectra (Top) and emissive dissymmetry factor g_{lum} (Bottom) of PVP films, (b) the fluorescence region and (c) the phosphorescence region for *S*-ONPY, *S*-CNPY, *R*-ONPY, and *R*-CNPY, respectively, at room temperature.

Figure 4a shows the normalized prompt and delayed PL spectra at room temperature for PY, ONPY, and CNPY PVP films. Similar to those observed in solutions at 77 K, these films also exhibit intense blue fluorescence at 360-500 nm and red phosphorescence at 570-800 nm, as illustrated by the inset pictures in Figure 4a and the CIE coordinates in Figure S8, ESI†. In detail, the fluorescence and phosphorescence emissions of both ONPY and CNPY are derived from the pyrene segments with the corresponding energy levels and vibrational features maintained. The lifetimes (Figure S7, ESI†) and PL quantum

yields (up to 69.6%, Figure S9, ESI†) are also included, suggesting ultrabright PVP films with impressive red afterglow.

To deepen the understanding of excited-state relaxation processer, we calculated the photophysical parameters for PY, CNPY, and ONPY, as shown in Table S2, ESI†. The results indicate that the intersystem crossing rate (k_{ISC}) of CNPY (1.50×10^7 s^{-1}) and ONPY (1.63×10^7 s^{-1}) is one to two orders of magnitude higher than that of pure pyrene (6.49×10^5 s^{-1}), which confirms that the binaphthalene axial chiral scaffold effectively boosts the ISC efficiency of pyrene. In addition, the phosphorescence rate constant (k_P) of CNPY/ONPY is significantly lower than that of pyrene, while the non-radiative transition rate (k_{NR}(T-S)) is basically same, which indicates that effective intermolecular interactions suppress the non-radiative decay from the triplet excited states of their pyrene moieties, and the extended π-conjugation in ONPY and CNPY endows them with a more prominent $^3(\pi,\pi^*)$ character in T_1, thus yielding a longer phosphorescence lifetime in comparison with pyrene.

The CPL behaviours of the PVP films exhibit the same trend as observed in solutions. The CPL intensity exhibited a distinct enhancement with the molecular architecture transitioning from the open to the locked structure, with the $|g_{lum}|$ in CPF of CNPY enantiomers reaching 7.4×10^{-3}, which is approximately twice that of ONPY enantiomers (Figure 4b). Furthermore, a detectable CPP signal with a $|g_{lum}|$ of 6.5×10^{-3} was observed exclusively for CNPY enantiomers, whereas the CPP signal of ONPY was almost negligible (Figure 4c). Furthermore, it also calculated another parameter, FM, which characterizes the overall performance of CPL. CNPY enantiomers has a higher FM value compared to that of ONPY enantiomers[57-59] (Table S3, ESI†). Collectively, these phenomena corroborate the effectiveness of the strategy of locking axial chirality scaffolds, which suppresses conformational freedom and mediates transition dipole moments, facilitating CPL.

Conclusions

In conclusion, this work demonstrates an effective strategy for achieving efficient circularly polarized luminescence and red circularly polarized phosphorescence in pyrene derivatives by manipulating a locked axial chiral scaffold. The structure-property relationship clearly demonstrates that introducing the chiral binaphthalene scaffold and locking its axial chirality are crucial for tailoring the luminescent properties of the pyrene moiety. Mediated by the transient triplet excited states of the binaphthalene unit, the overall intersystem crossing process is boosted. Combined with the enhanced molecular rigidity and optimized dipole moments, remarkably, the CNPY enantiomers doped into PVP achieve bright circularly polarized luminescence with a $|g_{lum}|$ of 7.4×10^{-3} and a Φ_{PL} of 65.7%, as well as distinct red circularly polarized phosphorescence with a $|g_{lum}|$ of ~6.5×10^{-3} and τ_P of 381.9 ms. This work provides a new design principle for developing efficient CPL and red CPP materials.

Author contributions

W.H. and C.W. performed all photophysical measurements, analysed data, synthesized materials, and performed theoretical calculations. M.W. assisted in characterizing molecular structure. Z.H. and Q.Z. designed and supervised the research. All authors discussed the results and commented on the manuscript.

Conflicts of interest

There are no conflicts to declare.

Data availability

The data that support the findings of this study are available from the corresponding author upon reasonable request.

Acknowledgements

The authors acknowledge the financial support from the National Natural Science Foundation of China (No. 22375054 and No. 21975061), the Natural Science Foundation of Guangdong Province (No. 2024B15150200960), the Shenzhen Fundamental Research Program (No. JCYJ20241202152659001 and No. GXWD20231130104319001), the China Postdoctoral Science Foundation (No. 2025M784345) and the Postdoctoral Fellowship Program (Grade C) of the China Postdoctoral Science Foundation (No. GZC20252722). The authors thank Prof. Dr. Lijuan Song (Harbin Institute of Technology, Shenzhen) for support with the computing platform and Prof. Dr. Zujin Zhao (South China University of Technology) for support with the chiral optical characterization device.

References

1. D. Liu, W.-J. Wang, P. Alam, Z. Yang, K. Wu, L. Zhu, Y. Xiong, S. Chang, Y. Liu, B. Wu, Q. Wu, Z. Qiu, Z. Zhao and B. Z. Tang, Highly efficient circularly polarized near-infrared phosphorescence in both solution and aggregate, *Nat. Photonics*, 2024, **18**, 1276-1284.
2. Y. Zhang, D. Li, Q. Li, Y. Quan and Y. Cheng, High Comprehensive Circularly Polarized Electroluminescence Performance Improved by Chiral Coassembled Host Materials, *Adv. Funct. Mater.*, 2023, **33**, 2309133.
3. M. Zeng, W. Wang, S. Zhang, Z. Gao, Y. Yan, Y. Liu, Y. Qi, X. Yan, W. Zhao, X. Zhang, N. Guo, H. Li, H. Li, G. Xie, Y. Tao, R. Chen and W. Huang, Enabling robust blue circularly polarized organic afterglow through self-confining isolated chiral chromophore, *Nat. Commun.*, 2024, **15**, 3053.
4. C. Yin, S. Sun, Z.-A. Yan, H. Hu, P. Jiang, Z. Xu, H. Tian and X. Ma, A universal strategy for multicolor organic circularly polarized afterglow materials with high dissymmetry factors, *Proc. Natl. Acad. Sci.*, 2025, **122**, e2419481122.
5. S. An, L. Gao, A. Hao and P. Xing, Ultraviolet Light Detectable Circularly Polarized Room Temperature Phosphorescence in Chiral Naphthalimide Self-Assemblies, *ACS Nano*, 2021, **15**, 20192-20202.
6. S. Garain, A. A. Kongasseri, S. M. Wagalgave, R. Konar, D. Deb, K. S. Narayan, P. K. Samanta and S. J. George, Supramolecular Charge‐Transfer Approach for Tunable

and Efficient Circularly Polarized Delayed Fluorescence and Phosphorescence, *Angew. Chem. Int. Ed.*, 2025, **64**, e202501330.

7. Z. Gao, X. Yan, Q. Jia, J. Zhang, G. Guo, H. Li, H. Li, G. Xie, Y. Tao and R. Chen, Stimulating Chiral Selective Expression of Room Temperature Phosphorescence for Chirality Recognition, *Adv. Sci.*, 2024, **11**, 2410671.
8. J. Xia, C. Xiong, S. Mo, Y. Zhang, K. Zhang, G. Li, J. Shi, J. Zhi, B. Tong, Q. Wu, P. Sun, Z. Cai and Y. Dong, Near-infrared circularly polarized organic room temperature phosphorescence based on a chiral host–guest doping strategy, *J. Mater. Chem. C*, 2024, **12**, 9578-9585.
9. W. Hao, Y. Wang and M. Liu, Nonaromatic lysine supramolecular nanotube assemblies with excitation-dependent circularly polarized phosphorescence, *ACS Mater. Lett.*, 2024, **6**, 3487-3495.
10. J. Liu, X. Y. Zhou, J. Wei, J. J. Wu, J. X. Hu, X. Y. Fang, R. C. Lan, Y. Tao, Y. Ma, B. X. Li, H. Yang, Y. Q. Lu and Q. Zhao, Multi‐Color Circularly Polarized Room‐Temperature Phosphorescence from Processable Chiral Photonic Films, *Adv. Funct. Mater.*, 2025, **35**, 2506911.
11. Z. P. Song, J. Wei, J. Liu, Z. F. Chu, J. X. Hu, S. Chakraborty, Y. Ma, B. X. Li, Y. Q. Lu and Q. Zhao, Mechanically‐Tunable and Full‐Color Circularly Polarized Long‐Lived Phosphorescence in Chiral Superstructure Elastomers, *Adv. Mater.*, 2025, **37**, 2419640.
12. X. Zou, N. Gan, Y. Gao, L. Gu and W. Huang, Organic Circularly Polarized Room-Temperature Phosphorescence: Strategies, Applications and Challenges, *Angew. Chem. Int. Ed.*, 2025, **64**, e202417906.
13. J. Liu, X. Zhou, X. Tang, Y. Tang, J. Wu, Z. Song, H. Jiang, Y. Ma, B. Li, Y. Lu and Q. Li, Circularly Polarized Organic Ultralong Room-Temperature Phosphorescence: Generation, Enhancement, and Application, *Adv. Funct. Mater.*, 2025, **35**, 2414086.
14. X. Wang, S. Ma, B. Zhao and J. Deng, Frontiers in Circularly Polarized Phosphorescent Materials, *Adv. Funct. Mater.*, 2023, **33**, 2214364.
15. S. Qiu, W. Li, S. Zhang, W. Xu, J. Tang, W. Tian and H. Wang, C3‐symmetric Triple Thia/Sulfone[6]Helicene with Dual Emissions, *Chem. - Eur. J.*, 2025, **31**, e202500554.
16. S. Tanaka, D. Sakamaki, N. Haruta, T. Sato, M. Gon, K. Tanaka and H. Fujiwara, A double heterohelicene composed of two benzo[b]phenothiazine exhibiting intense room-temperature circularly polarized phosphorescence, *J. Mater. Chem. C*, 2023, **11**, 4846-4854.
17. W. Gong, M. Zhou, L. Xiao, C. Fan, Y. Yuan, Y. Gong and H. Zhang, Multicolor‐Tunable and Time‐Dependent Circularly Polarized Room‐Temperature Phosphorescence from Liquid Crystal Copolymers, *Adv. Opt. Mater.*, 2023, **12**, 2301922.
18. S. Zhao, Y. Wen, Z. Yang, H. He, H. Liu and B. Yang, n/π Orbital Decoupling via Heavy Selenium Atoms toward Efficient Red Room-Temperature Phosphorescence in Purely Organic Systems, *J. Am. Chem. Soc.*, 2025, **147**, 43029-43040.
19. W. Huang and Z. He, Initialing Circularly Polarized Room-Temperature Phosphorescence from Purely Organic Luminophore Aggregate, *Synlett*, 2023, **34**, 2249-2256.
20. L. Guang, Y. Lu, Y. Zhang, R. Liao and F. Wang, Circularly Polarized Phosphorescence of Benzils Achieved by Chiral Supramolecular Polymerization, *Angew. Chem. Int. Ed.*, 2024, **63**, e202315362.
21. W. Huang, Y. Zhu, K. Zhou, L. Chen, Z. Zhao, E. Zhao and Z. He, Boosting Circularly Polarized Luminescence from Alkyl-Locked Axial Chirality Scaffold by Restriction of Molecular Motions, *Chem. - Eur. J.*, 2024, **30**, e202303667.
22. W. Huang, C. Fu, Z. Liang, K. Zhou and Z. He, Strong Circularly-Polarized Room-Temperature Phosphorescence from a Feasibly Separable Scaffold of Bidibenzo[b,d]furan with Locked Axial Chirality, *Angew. Chem. Int. Ed.*, 2022, **61**, e202202977.
23. H. Wang, W. Zhang, J. Huang, Y. Zhang, H. Li, L. Huang, W. Li, F. Zhang and G. Qing, Ultra-Stable, Long-Lived, and Multicolor Circularly Polarized Room-Temperature Phosphorescence Enabled by Shrimp-Derived Chitosan Nanocomposite Chemistry, *Adv. Funct. Mater.*, 2025, e27613.
24. J. You, R. Tian, C. Yin, J. Wang, J. Zhang and J. Zhang, Organic Circularly Polarized Room-Temperature Phosphorescence Toolbox with Excellent Practicality and Functionality, *ACS Nano*, 2025, **19**, 38219-38230.
25. L. Jin, W. Mo, Z. Wang and W. Hong, Vortex-Enabled Nonreciprocal Circularly Polarized Luminescence in Achiral Polymer Systems, *Adv. Funct. Mater.*, 2025, **36**, e21524.
26. C. Liu, L. Liu, Y. Song, G. Tian and Y. Cheng, Color-Tunable Circularly Polarized Room-Temperature Phosphorescence by Intermolecular Phosphorescence Resonance Energy Transfer in a Chiral Co-assembled Liquid Crystal Polymer Network, *J. Phys. Chem. Lett*, 2025, **16**, 9568-9576.
27. N. Su, J. Wang, Y. Yang, Z. Yan, L. Zhou, Y.-X. Zheng and J. Ding, Chiral Single Molecule with Biphenyl Component Exhibiting Both TADF and RTP Emissions Enables Highly Efficient CP-OLEDs, *Angew. Chem. Int. Ed.*, 2025, **64**, e202512717.
28. B. Yang, S. Yan, S. Ban and W. Huang, New horizons in phosphorus-based emitters: From circularly polarized fluorescence to room-temperature phosphorescence, *Chin. Chem. Lett.*, 2025, **36**, 110837.
29. P. Tao, J. Jin, X. Zheng, Y.-J. Pu and W.-Y. Wong, Engineering emissive excited states in organic electroluminescent materials, *Matter*, 2025, **8**, 102142.
30. M. M. Islam, Z. Hu, Q. Wang, C. Redshaw and X. Feng, Pyrene-based aggregation-induced emission luminogens and their applications, *Mater. Chem. Front.*, 2019, **3**, 762-781.
31. J. Zhao, S. Shi, X. Zhang, D. Liu, F. Song, Y. Cheng and F. Li, Circularly polarized luminescence pyrene materials: From design to applications, *Coord. Chem. Rev.*, 2026, **548**, 217173.
32. Z. Wang, L. Gao, Y. Zheng, Y. Zhu, Y. Zhang, X. Zheng, C. Wang, Y. Li, Y. Zhao and C. Yang, Four-in-One Stimulus-Responsive Long-Lived Luminescent Systems Based on Pyrene-Doped Amorphous Polymers, *Angew. Chem. Int. Ed.*, 2022, **61**, e202203254.
33. A. Cheng, H. Su, X. Gu, W. Zhang, B. Zhang, M. Zhou, J. Jiang, X. Zhang and G. Zhang, Disorder-Enhanced Charge-Transfer-Mediated Room-Temperature Phosphorescence in Polymer Media, *Angew. Chem. Int. Ed.*, 2023, **62**, e202312627.
34. Y. S. Lee, H. Nam, Y. N. Song, W. P. Hong, W.-S. Han and T. Kim, Simultaneous exciton control and electron recycling in pyrene-based stable blue fluorescent organic light-

emitting diodes via hybridized local and charge transfer and triplet-triplet fusion mechanisms, *Chem. Eng. J.*, 2025, **521**, 166658.

35. W. Feng, D. Chen, Y. Zhao, B. Mu, H. Yan and M. Barboiu, Modulation of Deep-Red to Near-Infrared Room-Temperature Charge-Transfer Phosphorescence of Crystalline "Pyrene Box" Cages by Coupled Ion/Guest Structural Self-Assembly, *J. Am. Chem. Soc.*, 2024, **146**, 2484-2493.
36. Y. Yan, Z. Ye, X. Qi, W. Xie, Y. Zhao, Y. Shangguan, T. Lin, Q. Chen, Y. Wang and J. Li, Pyrene-based red room-temperature phosphorescent guest-materials with high quantum yield and narrow emission peak, *Spectrochimica Acta Part A: Molecular and Biomolecular Spectroscopy*, 2026, **348**, 127109.
37. Y. Jiang, C. Zhang, R. Wang, Y. Lei, W. Dai, M. Liu, H. Wu, Y. Tao and X. Huang, Chiral‐Guest Induced Multicolor‐Tunable Circularly Polarized Room Temperature Phosphorescence, *Adv. Opt. Mater.*, 2023, **12**, 2302482.
38. L.-T. Bao, R.-H. Zhang, X. Yuan, X. Wang, P. Wu, X.-Q. Wang, J. Chen, A. Zhu, H.-B. Yang and W. Wang, Rigidly Locked Pyrene Excimers in Planar Chiral Pyrenophanes for Intense and Stable Circularly Polarized Photoluminescence and Electrochemiluminescence, *Angew. Chem. Int. Ed.*, 2025, **64**, e202500472.
39. X. Wang, P. Wu, Y. Wang, T. Cui, M. Jia, X. He, W. Wang, H. Pan, Z. Sun, H.-B. Yang and J. Chen, Unraveling the Origin of Multichannel Circularly Polarized Luminescence in a Pyrene-Functionalized Topologically Chiral [2]Catenane, *Angew. Chem. Int. Ed.*, 2024, **63**, e202407929.
40. J.-L. Song, C. Chen, X. Li, Y. Jiang, Z. Peng, X.-Q. Wang, H.-B. Yang and W. Wang, Boosting the circularly polarized luminescence of pyrene-tiaraed pillararenes through mechanically locking, *Nat. Commun.*, 2024, **15**, 10531.
41. Z. Xie, J. Deng, D. Liu, J. Lin, T. Jiang, X. Wang, W. Liu, L. Ma, F. Song, Z. Xiong, J. Chen, J. Zhang, C. Redshaw, Z. Zhao, X. Feng and B. Z. Tang, Unlocking intrinsically chiral bipyrenyl-based aggregation-induced emission luminogens: circularly polarized luminescence and dynamic chirality amplification, *Chem. Sci.*, 2026, **17**, 4145-4156.
42. X. Wang, K. Yang, B. Zhao and J. Deng, Polymeric Cholesteric Superhelix Induced by Chiral Helical Polymer for Achieving Full‐Color Circularly Polarized Room‐Temperature Phosphorescence with Ultra‐High Dissymmetry Factor, *Small*, 2024, **20**, 2404576.
43. L. Wang, A. Hao and P. Xing, Steroid-Aromatics Clathrates as Chiroptical Materials with Circularly Polarized Luminescence and Phosphorescence, *ACS Appl. Mater. Interfaces*, 2022, **14**, 44902-44908.
44. X. Wang, Q. Miao, W. Zhang, Y. Zhou, R. Xiong, Y. Duan, X. Meng and C. Ye, Switchable circular polarized phosphorescence enabled by cholesteric assembled nanocelluloses, *Chem. Eng. J.*, 2024, **481**, 148463.
45. S. Huang, Q. Wu, R. Luo, B. Tan, Y. Yuan and H. Zhang, Tunable Helix Inversion and Circularly Polarized Luminescence in Cholesteric Liquid Crystal Copolymers with Room-Temperature Phosphorescence, *Macromolecules*, 2024, **57**, 9017-9029.
46. Y. Gao, W. Ye, K. Qiu, X. Zheng, S. Yan, Z. Wang, Z. An, H. Shi and W. Huang, Regulating Isolated-Molecular and Aggregated-State Phosphorescence for Multicolor Afterglow by Photoactivation, *Adv. Mater.*, 2023, **35**, 2306501.
47. G. Yang, J. Li, X. Deng, X. Song, M. Lu, Y. Zhu, Z. Yu, B. Xu, M.-D. Li and L. Dang, Construction and Application of Large Stokes-Shift Organic Room Temperature Phosphorescence Materials by Intermolecular Charge Transfer, *J. Phys. Chem. Lett*, 2023, **14**, 6927-6934.
48. T. Z. Sodia, K. E. Frank, A. A. Mendonsa, J. M. Branning, Jr. and K. J. Cash, Coupling Organic Ultralong Lifetime Phosphorescence Materials with Paper-Based Bioanalytical Architectures for Autofluorescence-Free Sensing, *ACS Sens.*, 2025, **10**, 4873-4881.
49. K. Li, C. Fu, H. Yamagishi, S. Nakayama, W. Y. Heah, Y. Cheng, R. Oda, W. Yospanya and Y. Yamamoto, Microscopic observations of RGB circularly polarized luminescence from solid microspheres with liquid crystalline molecular order, *Sci. Technol. Adv. Mater.*, 2025, **26**, 2509486.
50. Q. G. He, Z. Z. Chu, G. T. Lei, A. J. Qin, H. Z. Lin, F. L. Bai, J. G. Cheng and Y. Qiu, A pure blue light emitting binaphthyl derivative: Synthesis and properties, *Chin. Chem. Lett.*, 2008, **19**, 431-434.
51. X. Feng, X. Wang, C. Redshaw and B. Z. Tang, Aggregation behaviour of pyrene-based luminescent materials, from molecular design and optical properties to application, *Chem. Soc. Rev.*, 2023, **52**, 6715-6753.
52. W. Zhao, T. S. Cheung, N. Jiang, W. Huang, J. W. Y. Lam, X. Zhang, Z. He and B. Z. Tang, Boosting the efficiency of organic persistent room-temperature phosphorescence by intramolecular triplet-triplet energy transfer, *Nat. Commun.*, 2019, **10**, 1595.
53. L. Xiao, Z. Wang, C. Zhang, X. Xie, H. Ma, Q. Peng, Z. An, X. Wang, Z. Shuai and M. Xiao, Long Persistent Luminescence Enabled by Dissociation of Triplet Intermediate States in an Organic Guest/Host System, *J. Phys. Chem. Lett*, 2020, **11**, 3582-3588.
54. B. Wu, H. Su, A. Cheng, X. Zhang, T. Wang and G. Zhang, The El-Sayed's rule analogy enables long-lived room temperature phosphorescence in twisted biphenyls, *Cell Rep. Phys. Sci.*, 2023, **4**, 101245.
55. X. Li, W.-T. Xu, X.-Q. Xu, Y. Wang, X.-Q. Wang, H.-B. Yang and W. Wang, Lighting Up Bispyrene-Functionalized Chiral Molecular Muscles with Switchable Circularly Polarized Excimer Emissions, *Angew. Chem. Int. Ed.*, 2025, **64**, e202412548.
56. R. Benny, N. Kumar, A. Bera, R. Srithar, S. Pramanik, S. Reddy Vennapusa and S. De, Controlling the Chiroptical Properties of Pyrene-Based Tweezers by Conformation Locking, *ChemPhotoChem*, 2025, **9**, e202400396.
57. H. Lu, L. Di Bari and L. Favereau, Standardizing the characterization of circularly polarized luminescence of chiral materials, *Nat. Photonics*, 2025, **19**, 1041-1047.
58. L. Yao, G. Niu, J. Li, L. Gao, X. Luo, B. Xia, Y. Liu, P. Du, D. Li, C. Chen, Y. Zheng, Z. Xiao and J. Tang, Circularly Polarized Luminescence from Chiral Tetranuclear Copper(I) Iodide Clusters, *J. Phys. Chem. Lett*, 2020, **11**, 1255-1260.
59. L. Arrico, L. Di Bari and F. Zinna, Quantifying the Overall Efficiency of Circularly Polarized Emitters, *Chem. - Eur. J.*, 2021, **27**, 2920-2934.

View Article Online
DOI: 10.1039/D6SC01341D

The data supporting this article have been included as part of the Supplementary Information.